

In vitro and *in silico* characterization of open-cell structures of trabecular bone

S. J. Ramos-Infante and M. A. Pérez

M2BE-Multiscale in Mechanical and Biological Engineering, Instituto de Investigación en Ingeniería de Aragón (I3A), Universidad de Zaragoza Campus Río Ebro, Zaragoza, Spain

ABSTRACT

This work aimed to perform a detailed *in vitro* and *in silico* characterization of open-cell structures, which resemble trabecular bone, to elucidate osteoporosis failure mechanisms. Experimental and image-based computational methods were used to estimate Young's modulus and porosities of different open-cell structures (Sawbones; Malmö, Sweden). Three different open-cell structures with different porosities were characterized. Additionally, some open-cell structures were scanned using a microcomputed tomography system (μ CT) to non-destructively predict specimen Young's modulus of the structures by developing voxel-based and tetrahedral finite element (FE) models. A 3D reconstruction and FE analyses were used. The experimental and computational results with different element types (linear and quadratic tetrahedrons and voxel-based meshes) were compared with Sawbones data (Sawbones; Malmö, Sweden) revealing important differences in Young's modulus and porosities. The specimens with high and low volume fractions were best represented by linear and quadratic tetrahedrons, respectively. These results could be used to develop new osteoporosis-prevention strategies.

ARTICLE HISTORY

Received 21 August 2017
Accepted 5 October 2017

KEYWORDS

Micro-CT data; open-cell structures; voxel meshes; tetrahedral meshes; *in vitro* and *in silico* compressive tests

1. Introduction

Bone strength reflects the integration of two main features: bone mineral density, expressed as grams of mineral per area/volume, and bone quality, which consists of bone architecture, turnover, damage accumulation, collagen cross-linking, and bone mineralization (Cowin 1989). In combination with cortical bone, trabecular bone is a major load-bearing biological tissue in human bone. Trabecular bone is involved in bone femur fractures and is the primary site for the insertion of orthopaedic implants (Eswaran et al. 2006). Substantial direct and indirect social and economic costs are associated with these fractures, which emphasize the need for the prevention and treatment of osteoporotic disease (Daszkiewicz et al. 2017). Osteoporosis is now recognized as a major public health problem facing postmenopausal women and ageing individuals irrespective of gender (Stauber et al. 2014). In fact, osteoporosis is a widespread skeletal disease that is responsible for deleterious fractures (Hamblin 2013). In this context, *in silico* medicine may prove useful (Viceconti et al. 2015).

Because bone is anisotropic, it is particularly difficult to handle in finite element analysis (FEA) involving

cancellous bone as the trabecular struts themselves run in different directions. The properties of cancellous bone vary greatly as a function of their apparent density. For cancellous bone, the elastic compressive modulus at 75% porosity is approximately around 160 MPa, which is close to the human bone trabecular compressive modulus (Pioletti 2010).

Many computational models to predict the mechanical properties of trabecular bone have been developed. For instance, the elastic behaviour of trabecular bone was studied using several different approaches, involving analytical and computational techniques. Analytical studies represent trabecular bone as a cellular solid and express its Young's modulus by power law relations in terms of density (Gibson and Ashby 1982; Gibson 1985; Rajan 1985; Gibson and Ashby 1999; Gibson et al. 2010, 1982). Although density is a key parameter in determining the properties of trabecular bone, density alone cannot fully capture the mechanical behaviour of bone. Other researchers have defined a fabric tensor, which characterizes the textural or structural anisotropy of trabecular bone, and described the relationships between the elastic constants of trabecular bone and its fabric tensor and density (Turner et al. 1990; Kabel et al. 1999; Zysset 2003).

CONTACT S. J. Ramos-Infante  sramos@unizar.es

© 2017 The Author(s). Published by Informa UK Limited, trading as Taylor & Francis Group. This is an Open Access article distributed under the terms of the Creative Commons Attribution-NonCommercial-NoDerivatives License (<http://creativecommons.org/licenses/by-nc-nd/4.0/>), which permits non-commercial re-use, distribution, and reproduction in any medium, provided the original work is properly cited, and is not altered, transformed, or built upon in any way.

Trabecular bone architecture, which is characterized by the thickness, number and separation distance of individual trabecula as well as their three-dimensional connectivity, plays an important role in its response. Thus, high-resolution imaging techniques, that account for actual trabecular bone architecture, such as micro-computed tomography (μ CT), were used in combination with the finite element method (FEM) to predict Young's modulus of trabecular bone (Müller and Rüegegger 1995; Ulrich et al. 1998; Bourne and van der Meulen 2004; Dobson et al. 2006; Follet et al. 2007; Harrison et al. 2008; Pahr and Zysset 2008). Generally, finite element (FE) models of bones may be categorized into two groups: micro-finite element (μ FE) models, in which the trabecular bone morphology is modelled in detail (Homminga et al. 2004; Verhulp et al. 2006; Fields et al. 2009; Nawathe et al. 2013), and homogenized continuum-level (hFE) models, in which one element covers a larger bone region, which is considered a homogeneous material (Faulkner et al. 1991; Martin et al. 1998; Pistoia et al. 2001; Crawford et al. 2003; Imai et al. 2006; Schileo et al. 2007; Pahr and Zysset, 2009; Pahr et al. 2012). hFE models have been used for diverse clinical applications such as predicting bone strength (Zysset et al. 2013) and mechanical properties (van Rietbergen et al. 1995), but meshing (Viceconti et al. 1998; Treece et al. 1999; Ito et al. 2006) and material mapping (Pahr and Zysset, 2009; Taddei et al. 2007) may be challenging. The limitations of quantitative morphometry for the prediction of bone failure have been demonstrated in previous studies, which showed that the strength of trabecular bone specimens depends on the orientation of the applied load (Bevill et al. 2009; Parkinson et al. 2012) and on local variations in the trabecular network (Perilli et al. 2008). From a geometric or mesh point of view, one can distinguish between voxel-mesh (Keyak et al. 1997; Crawford et al. 2003; Dall'Ara et al. 2013) and smooth mesh geometries (linear tetrahedral and quadratic tetrahedral) (Jones and Wilcox 2007; Yosibash et al. 2010; Luisier et al. 2014; Zysset et al. 2015). Although these elements are normally used in full-bone meshes (Pahr and Zysset 2016), it would be interesting to observe the effects of these element types on the prediction of the mechanical properties of trabecular bone.

Indeed, trabecular bone plays an important role in load transmission and energy absorption at major joints such as the knee, hip, and spine. It is believed that, in addition to the bone volume fraction (the ratio of the volume of bone tissue to the overall bulk volume), the detailed microarchitecture, including trabecular orientation and connectivity, is important in governing the mechanical properties of trabecular bone (Wang et al. 2015). For this reason, efforts to quantify structural properties have gained prominence, and many different

methods have been proposed to further describe the influence of changes in bone microstructure on bone mechanical properties (Hildebrand and Rüegegger 1997; Jinnai et al. 2002; Gomberg et al. 2003; Zysset 2003). It is also possible that heterogeneity may locally weaken the trabecular bone structure and ultimately initiate failure. This possibility casts doubt on the reliability of failure prediction based on average morphometric indices and the appropriate interpretation of the mechanical results from compression testing (Stauber et al. 2014).

The structure of open-cell rigid foams resembles that of human cancellous bone. The cell structure is over 95% open and the cell size ranges from 1.5 to 2.5 mm. Furthermore, these foams are suitable for a variety of applications that require an open-cell structure, such as dynamic testing or cement injection, prior to clinical purposes. Therefore, this study involved *in vitro* and *in silico* characterization of commercial open-cell structures to quantify the influence of voxel-mesh and smooth mesh geometries for the prediction of the mechanical properties of trabecular bone. Our results will reveal new research strategies to prevent osteoporotic fractures. To achieve this goal, Young's modulus was compared between three commercial open-cell structures (Sawbones; Malmö, Sweden) with different porosities to assess the best element type that represents trabecular bone microarchitecture (linear tetrahedral, quadratic tetrahedral or voxel). A 3D reconstruction from μ CT images was performed and μ FE models were developed using MIMICS (Materialise NV, Leuven, Belgium). Subsequently, the computationally estimated Young's modulus and porosity results were compared with the experimental and commercial Sawbones data.

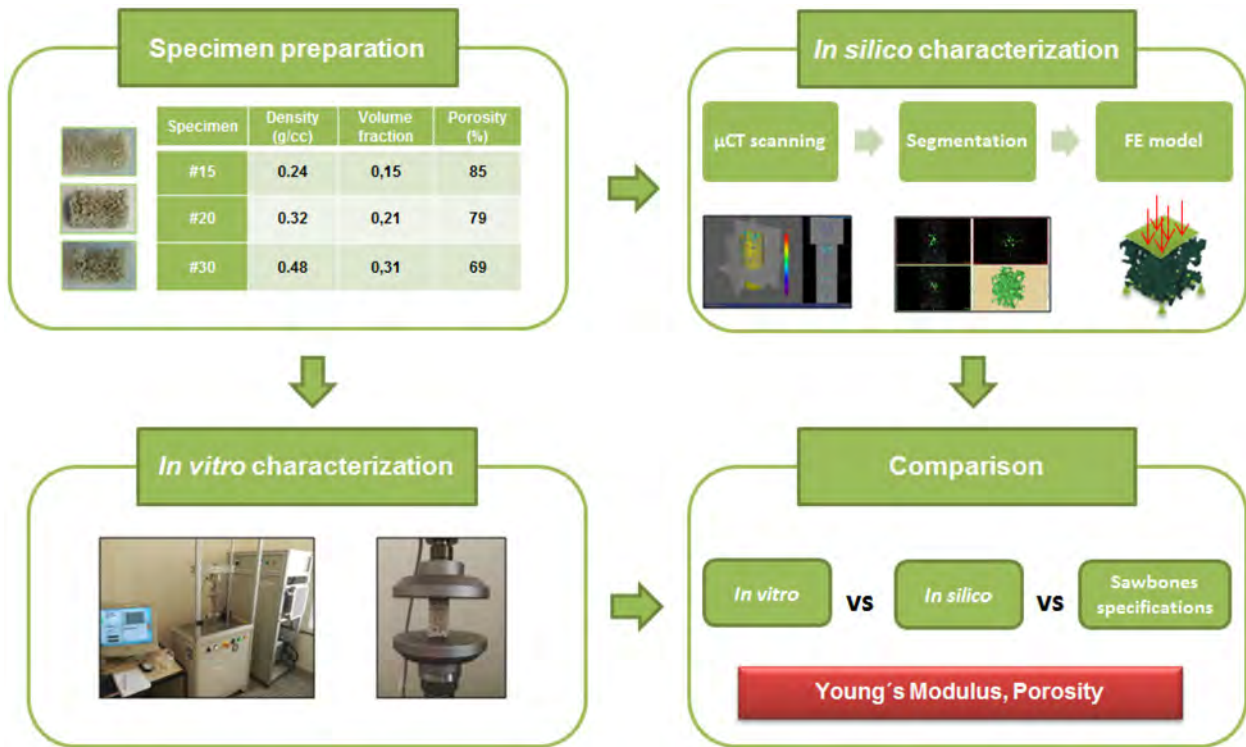
2. Materials and methods

Three different open-cell structures were studied (Sawbones; Malmö, Sweden) (Table 1). Henceforth, we will refer to these as specimen #30 (Sawbones, product No. 1522–525; Malmö, Sweden; Figure 1), specimen #20 (Sawbones, product No. 1522–524; Malmö, Sweden; Figure 1) and specimen #15 (Sawbones, product No. 1522–526-1; Malmö, Sweden; Figure 1). Their densities resembled trabecular bone and varied from 0.24 to 0.48 g/cm³ (Table 1). We had 53 cubic specimens (17 of specimen #15, 18 of specimen #20 and 18 of specimen #30) (Figure 1). First, an *in silico* characterization was performed to simulate the experimental compressive test. Then, an *in vitro* characterization was performed (Figure 1).

Both results were compared with Sawbones specifications (Figure 1). The apparent Young's moduli and porosities were assessed.

Table 1. Open-cell specimen dimensions, densities, volume fractions and Young's modulus.

Specimen	Number of specimens	Density (g/cc)	Porosity specifications (%)	Young's modulus Sawbones specifications (MPa)	Base (mm)	Height (mm)	Thickness (mm)
#15	17	0.24	85	53	20	40	20
#20	18	0.32	79	105	20	40	20
#30	18	0.48	69	270	20	40	20

**Figure 1.** Workflow for the *in vitro* and *in silico* characterization of the open-cell structures of trabecular bone.

2.1. *In silico* characterization

First, among the 53 specimens only 18 (6 of each type) were scanned along their height with a microcomputed tomography system prior to the compression tests (μ CT50, General Electric; Milwaukee, WI, USA), using a 50- μ m nominal resolution to assess the architecture of the trabeculae. The scanned images were reconstructed using a semiautomatic reconstruction (MIMICS, Materialise NV; Leuven, Belgium). All specimens were also digitally cut to exclude bone fragments that might have been generated from the cutting process and to exclude unintentionally cut trabeculae. Therefore, the representative volume element (RVE) dimensions were 10 mm in base, 10 mm in height and 10 mm in thickness (10 \times 10 \times 10 mm).

The threshold μ CT images of trabecular bone were converted to μ FE models using the 3-Matic tooling module (Materialise NV; Leuven, Belgium) and the Voxel Create Mesh Module supplied by MIMICS (Materialise NV, Leuven, Belgium). After the mesh was constructed, the resulting μ FE models were imported into the commercial

FE software package ABAQUS v.6.14 (Dassault Systèmes Simulia Corp.; Suresnes, France).

Three mesh types were analysed. First, a voxel mesh based on the original μ CT images of trabecular bone (8-node brick element) was constructed. The voxel size was 12 μ m (Figure 2). Then, a linear tetrahedral mesh (mean element size: 25 μ m) and a quadratic tetrahedral mesh (mean element size: 25 μ m) were considered (Figure 2). The final tetrahedral mesh size was defined after mesh convergence analysis.

The bulk material was assumed to be linear elastic and isotropic. Therefore, the elements of the FE meshes were assigned a Young's modulus of 3200 MPa ($E_{\text{tissue}}^{\text{FE}}$). The Poisson's ratio was defined as 0.3. Previous mechanical properties were provided by Sawbones (Sawbones; Malmö, Sweden).

The boundary conditions for the μ FEM model were based on idealizations of those of a uniaxial compression test (Wang et al. 2015); a uniaxial displacement (strain of 2%) was applied to the top surface of the cubic bone

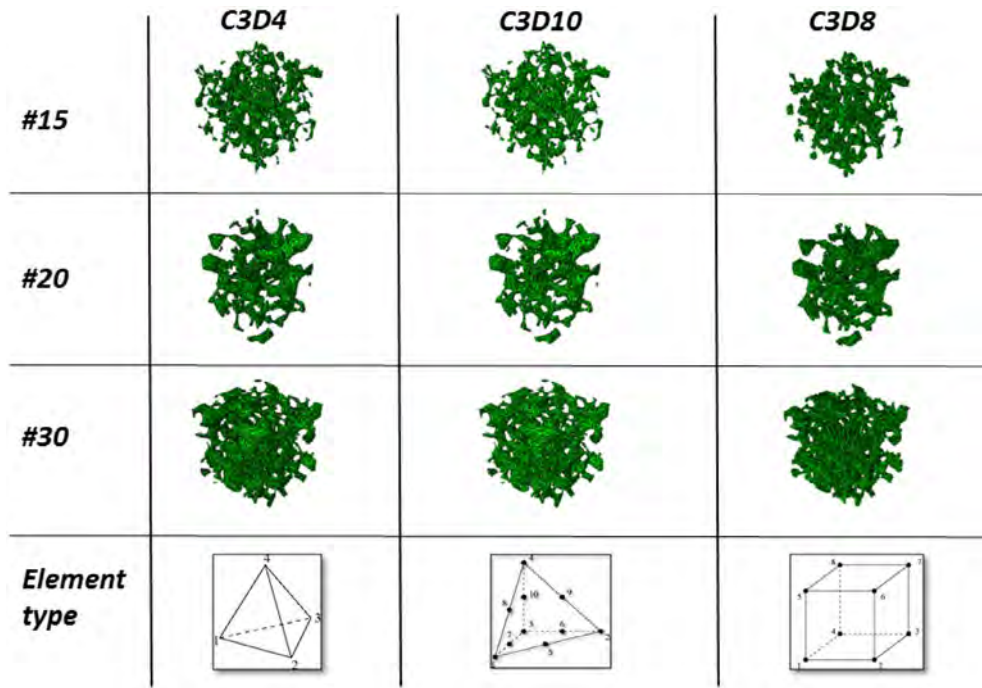


Figure 2. Three-dimensional reconstruction of the trabeculae using linear tetrahedral (C3D4), quadratic tetrahedral (C3D10) and voxel (C3D8) elements.

samples (Wang et al. 2015). The bottom surface was kept fixed (van Lenthe et al. 2006), and the sides were calculated as traction-free (Hamed et al. 2012) (Figure 1). In addition, contact between the upper and lower surfaces of the specimen and the plates was modelled using contact elements with a zero friction value to ensure that only compressive forces were transmitted (Hambli 2013).

Non-linear FE analyses were performed in ABAQUS v6.14 (Dassault Systèmes Simulia Corp.; Suresnes, France) and run in a computational cluster of 224 cores and 576 GB of RAM. After the FE analysis, the apparent Young's modulus (1) was calculated using the following equation:

$$E_{\text{app}}^{\text{Voxel}} = \frac{\sigma_{\text{app}}}{\epsilon_{\text{app}}} = \frac{F/A}{\Delta L/L} \quad (1)$$

in which F is the force calculated from each FE simulation (N), A is the apparent specimen cross-section (mm^2), $\Delta L = 0.2$ mm and L is the specimen length ($L = 10$ mm). Once the apparent Young's modulus was calculated, the apparent porosities ($P_{\text{app}}^{\text{Voxel}}$) were obtained using Equation (2), in which n was determined to be equal to 2 for an open-cell structure (Hamed et al. 2012):

$$P_{\text{app}}^{\text{Voxel}} = 1 - \sqrt[n]{\frac{E_{\text{app}}^{\text{Voxel}}}{E_{\text{tissue}}^{\text{FE}}}} \quad (2)$$

Furthermore, we could also calculate and compare the above mentioned porosities with the porosity associated with the specimen dimensions:

$$P_{\text{sp}} = \left(1 - \frac{V_{\text{app}}}{V}\right) \times 100 \quad (3)$$

where V_{app} is obtained from the FE material assignment module in MIMCS (Materialise NV; Leuven, Belgium) and V is the specimen volume size without pores ($V \approx 1000$ mm^3) obtained after the 3D specimen reconstruction.

2.2 In vitro characterization

Briefly, compression experiments were conducted using a servo-hydraulic material testing machine (Microtest, model EFH; Figure 1). Each specimen was placed between steel plates at room temperature (approx. 23 °C) and loaded in the direction of their axis of symmetry (Figure 1). The quasi-static compression load was measured with a commercial load cell (10 kN) applied at a constant velocity rate of 1 mm/min (Keaveny et al. 1993). Then, the force-displacement curves were measured for each test, and the Young's modulus was calculated.

3. Results

The experimental data clearly showed an increase in Young's modulus with bone volume fraction (Figure

3(a)). Furthermore, our experimental results for Young's modulus are close to the values provided by Sawbones (Sawbones; Malmö, Sweden) for specimen #15 and #20. In contrast, specimen #30 had a lower Young's modulus (Figure 3(a)) than the Sawbones specifications.

With regard to the apparent Young's modulus (Table 2), we observed that, depending on the mesh type used to perform the FEA, different values for the apparent Young's modulus could be obtained. For instance, the quadratic tetrahedral elements were more suitable for representing the real mechanical properties of the specimens that possessed lower volume fractions (Figure 3(a)) but also overestimated apparent Young's modulus. The use of quadratic tetrahedral elements resulted in a reduction in the inherent stiffness of linear tetrahedral elements. In contrast, linear tetrahedral elements were capable of representing the real mechanical properties of specimens with higher volume fractions (Figure 3) but underestimated the apparent Young's modulus. Similarly, we observed that regardless of the mesh type used to perform the FEA, for volume

fractions near 0.20 (Figure 3), the Young's modulus results and estimated porosity were similar to the real values. Despite these results, we found that the standard deviations seemed to increase as the volume fraction increased (Table 2).

With regard to estimated porosities (Table 3), large correlations between the estimated and real porosities were observed regardless of mesh type (Figure 3(b)). In addition, the mean porosities and standard deviations seemed to increase as the volume fraction increased (specimen #30). Nevertheless, the porosity results showed that linear tetrahedral elements were more suitable for representing the actual porosity of specimen #30.

4. Discussion

Anderson et al. (2007) outlined the major steps required to build a conceptual model that is a simplification of the actual conditions of interest and to then build a physical model (laboratory experiment) and a mathematical (FE)

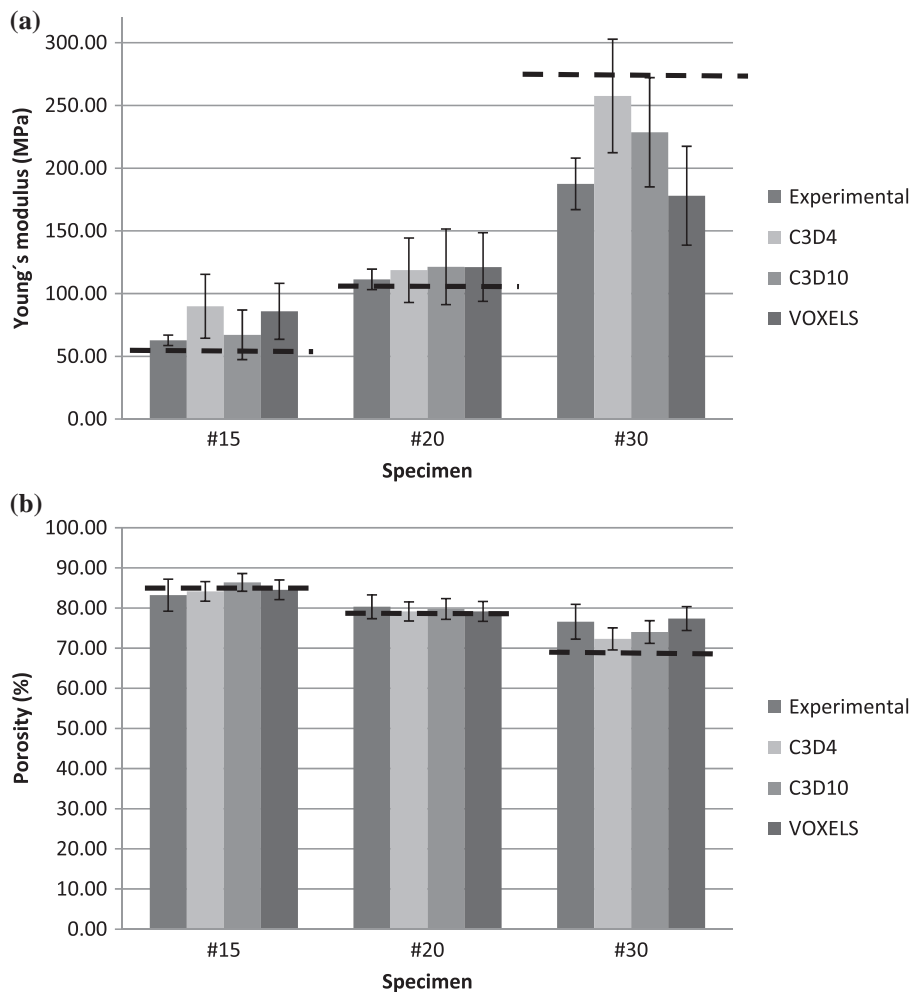


Figure 3. Comparison among experimental, computational and Sawbones specifications of (a) Young's modulus (MPa) and (b) porosity (the dashed line represents Sawbones specifications).

Table 2. Young's modulus (mean \pm SD) obtained experimentally and through three different finite element analyses.

Specimen	Dimensions (mm)	A_{app} (mm ²)	$E_{experimental}$ (MPa)	E_{app}^{lntet} (MPa)	$E_{app}^{quadtet}$ (MPa)	E_{app}^{Voxel} (MPa)
#15	10 \times 10 \times 10	15.39 \pm 3.20	62.74 \pm 4.14	89.93 \pm 5.45	67.15 \pm 19.82	85.89 \pm 22.33
#20	10 \times 10 \times 10	23.36 \pm 2.53	111.35 \pm 8.24	118.67 \pm 25.70	121.38 \pm 30.17	121.16 \pm 27.36
#30	10 \times 10 \times 10	26.18 \pm 2.70	187.47 \pm 20.53	257.57 \pm 45.29	228.58 \pm 43.55	178.05 \pm 39.44

Table 3. Estimated porosities (mean \pm SD) obtained experimentally and through three different finite element analyses.

Specimen	Dimensions (mm)	P_{sp} (%)	P_{app}^{lntet} (%)	$P_{app}^{quadtet}$ (%)	P_{app}^{Voxel} (%)
#15	10 \times 10 \times 10	83.21 \pm 3.98	84.15 \pm 2.44	86.38 \pm 2.21	84.55 \pm 2.44
#20	10 \times 10 \times 10	80.31 \pm 2.96	79.15 \pm 2.38	79.75 \pm 2.59	79.15 \pm 2.48
#30	10 \times 10 \times 10	76.59 \pm 4.34	72.30 \pm 2.75	74.02 \pm 2.81	77.38 \pm 2.99

model from the conceptual model. After testing and simulation, the results are compared, the uncertainties are analysed, and a statistical statement is formulated that determines whether the simulation model fits the experiment. Therefore, in this work, an *in vitro* and *in silico* characterization of open-cell structures of trabecular bone was performed.

Daszkiewicz et al. (2017) obtained a broad range of bone volume fraction (BV/TV) for the healthy femur of 0.242 ± 0.060 . Therefore, to accurately predict the mechanical properties of both healthy and osteoporotic cancellous bone, we used three different specimens of open-cell structures (Sawbones; Malmö, Sweden) (Figure 1) of the same size but different densities.

We obtained experimental and computational results through compression tests and μ FE analyses, respectively, of previous open-cell structures. A major strength of this study was the use of specimens with large variations in their microarchitecture and bone volume fraction for the experimental validation so that an accurate prediction of the mechanical properties of the artificial cancellous bone was achieved.

The gold standard for determining bone competence is an assessment of its mechanical properties in a functional mechanical test that determines the resultant stress and strain. (Burr 2016). First, experimental tests have been proposed to assess specimens. The experimental data clearly show an increase in Young's modulus with the bone volume fraction. Furthermore, our experimental results for Young's modulus are on the higher side but are on the lower side of the values provided by Sawbones (Sawbones; Malmö, Sweden) depending on the volume fraction. Hamed et al. (2012) showed that machining bone samples may cause significant surface defects that may result in a reduction in the mechanical properties of the specimen, that is, a reduction in Young's modulus (specimen #30). In fact, our initial specimens (20 \times 20 \times 40 mm) were cut from a larger specimen with a volume of 40 \times 40 \times 40 mm. Additionally, Dendorfer et al. (2008) showed that the accumulation of trabecular tissue damage and fracture

affects the induced force-displacement curve of the whole specimen. Furthermore, Hambli (2013) observed that in some cases, Young's modulus increases significantly because the progressive contact of the trabeculae generates compaction of the specimen microstructure (specimen #15). In fact, the loading rate plays an important role due to the stiffer behaviour bone exhibits when it is loaded at a higher rate, whereas bone that is loaded more slowly will appear to be less stiff (Burr 2016). Despite these limitations, our experimental results are in agreement with the mechanical properties provided by Sawbones (Sawbones; Malmö, Sweden).

Second, μ FE models were used and continue to be an important simulation tool. These models help interpret the results of mechanical tests and can reduce *in vitro* testing. However, we should take into account the numerical errors and uncertainties that occur with these methods (Ladd and Kinney 1998; Hamed et al. 2012). Therefore, in this paper, the effects of element type and element size and the effects of different specimen volume fractions were investigated. The results showed that the element type had some effects on the predicted yield behaviour. Due to the better bending behaviour for quadratic elements in specimen #15, the predicted Young's modulus were considerably lower than those obtained using linear elements (Verhulst et al. 2008). In contrast, specimens #20 and #30 showed better correlations for Young's modulus prediction with linear tetrahedral elements. A poor correlation was predicted using the voxel FE mesh for specimen #30. This result could be due to the substantial lack of connections during voxel meshing (Ulrich et al. 1998). Nevertheless, some simplifications in our model have been assumed, so further analysis is needed.

In the present study, we found that the variance in volume fraction in a single specimen can be relatively large (Stauber et al. 2014) due to the cutting process during specimen manufacture. Therefore, the first challenge is how to set a threshold value for μ CT images to accurately capture bone architecture and porosity. FE predictions of

the Young's modulus were already reported to be strongly affected by the threshold used for the segmentation of CT data to create the FE mesh (Hara et al. 2002) and are extremely sensitive to errors due to the power relationship between the volume fraction and mechanical properties (Chevalier et al. 2007). A finer resolution would better capture the trabecular bone architecture and lead to more accurate FE predictions. Another assumption is related to the constitutive behaviour of trabecular bone tissue. In this case, the non-linear nature of trabecular bone tissue has been simplified. This process can lead to errors due to modelling hypotheses and experimental errors in the compression test procedures (Keaveny et al. 1997), and in some cases, can lead to surprisingly low values for Young's modulus (Hou et al. 1998; Ladd and Kinney 1998). Finally, to avoid large computation time that can arise for more complex analyses, some authors (Niebur et al. 2000; Jaasma et al. 2002; Bayraktar and Keaveny 2004; Lü et al. 2015) have instead used smaller sub-regions, but this approximation was already said to result in errors as large as 9.5% in predictions of apparent stiffness (Bayraktar et al. 2004).

To summarize, our results indicate differences among the element type used for the FEA (linear tetrahedral vs. quadratic tetrahedral vs. voxel mesh). For instance, it could be concluded that quadratic tetrahedral elements were more suitable for representing the actual mechanical properties of specimens with lower volume fractions (high porous structures); that is, osteoporotic cancellous bone failure was able to be predicted using quadratic tetrahedral elements. In contrast, linear tetrahedral elements were capable of representing the real mechanical properties of specimens with higher volume fractions (low porous structures). Similarly, we observed that regardless of the mesh type used to perform the finite element analysis, both Young's modulus and estimated porosity were similar to the values in actual cases when the volume fractions were near 0.20. The use of linear and quadratic tetrahedral elements has not only allowed us to predict the mechanical properties of trabecular bone, but also led to a considerable reduction in computational costs.

A detailed *in vitro* and *in silico* characterization of open-cell structures was performed in this study. Our results will contribute to new strategies for osteoporotic fracture prevention that should be tested *in vitro* and supported by computational models.

Acknowledgements

The authors gratefully acknowledge the support the Spanish Ministry of Economy and Competitiveness through research project DPI 2014-53401-C2-1-R and the European Research Council (ERC) for supporting this work through project ERC-2012-stg306751. Also, the authors acknowledge the provision

of the compressive testing machine by Dr. Carlos Javierre from the University of Zaragoza.

Disclosure statement

No potential conflict of interest was reported by the authors.

Funding

This work was supported by Spanish Ministry of Economy and Competitiveness [grant number DPI 2014-53401-C2-1-R]; the European Research Council (ERC) [grant number ERC-2012-stg306751].

References

- Anderson AE, Ellis BJ, Weiss JA. 2007. Verification, validation and sensitivity studies in computational biomechanics. *Comput Methods Biomech Biomed Eng.* 10(3):171–184.
- Bayraktar HH, Keaveny TM. 2004. Mechanisms of uniformity of yield strains for trabecular bone. *J Biomech.* 37:1671–1678.
- Bayraktar HH, Morgan EF, Niebur GL, Morris GE, Wong EK, Keaveny TM. 2004. Comparison of the elastic and yield properties of human femoral trabecular and cortical bone tissue. *J Biomech.* 37:27–35.
- Bevill G, Farhamand F, Keaveny TM. 2009. Heterogeneity of yield strain in low-density versus high-density human trabecular bone. *J Biomech.* 42(13):2165–2170.
- Bourne BC, van der Meulen MC. 2004. Finite element models predict cancellous apparent modulus when tissue modulus is scaled from specimen CT-attenuation. *J Biomech.* 37(5):613–621.
- Burr DB. 2016. The use of finite element analysis to estimate the changing strength of bone following treatment for osteoporosis. *Osteoporos Int.* 27(9):2651–2654.
- Chevalier Y, Pahr D, Allmer H, Charlebois M, Zysset P. 2007. Validation of a voxel-based FE method for prediction of the uniaxial apparent modulus of human trabecular bone using macroscopic mechanical tests and nanoindentation. *J Biomech.* 40(15):3333–3340.
- Cowin SC. 1989. The mechanical properties of cortical bone tissue. Boca Raton (FL): CRC Press.
- Crawford RP, Cann CE, Keaveny TM. 2003. Finite element models predict *in vitro* vertebral body compressive strength better than quantitative computed tomography. *Bone* 33(4):744–750.
- Dall'Ara E, Luisier B, Schmidt R, Kainberger F, Zysset P, Pahr D. 2013. A nonlinear QCT-based finite element model validation study for the human femur tested in two configurations *in vitro*. *Bone* 52(1):27–38.
- Daszkiewicz K, Maquer G, Zysset PK. 2017. The effective elastic properties of human trabecular bone may be approximated using micro-finite element analyses of embedded volume elements. *Biomech Model Mechanobiol.* 16(3):731–742.
- Dendorfer S, Maier HJ, Taylor D, Hammer J. 2008. Anisotropy of the fatigue behaviour of cancellous bone. *J Biomech.* 41(3):636–641.
- Dobson CA, Sisiyas G, Phillips R, Fagan MJ, Langton CM. 2006. Three dimensional stereolithography models of cancellous bone structures from μ CT data: testing and validation of

- finite element results. *Proc Inst Mech Eng Part H. J Eng Med.* 220(3): 481–484.
- Eswaran SK, Gupta A, Adams MF, Keaveny TM. 2006. Cortical and trabecular load sharing in the human vertebral body. *J Bone Miner Res.* 21(2):307–314.
- Faulkner KG, Cann CE, Hasegawa BH. 1991. Effect of bone distribution on vertebral strength: assessment with patient-specific nonlinear finite element analysis. *Radiology* 179(3):669–674.
- Fields AJ, Eswaran SK, Jekir MG, Keaveny TM. 2009. Role of trabecular microarchitecture in whole-vertebral body biomechanical behavior. *J Bone Miner Res.* 24(9):1523–1530.
- Follet H, Peyrin F, Vidal-Salle E, Bonnassie A, Rumelhart C, Meunier PJ. 2007. Intrinsic mechanical properties of trabecular calcaneus determined by finite-element models using 3D synchrotron microtomography. *J Biomech.* 40(10):2174–2183.
- Gibson L. 1985. The mechanical behaviour of cancellous bone. *J Biomech.* 18(5):317–328.
- Gibson LJ, Ashby MF. 1982. The mechanics of three-dimensional cellular materials. *Proc Math Phys Eng Sci R Soc.* 382(1782):43–59.
- Gibson LJ, Ashby MF. 1999. *Cellular solids: structure and properties.* Cambridge: Cambridge University Press.
- Gibson LJ, Ashby MF, Schajer GS, Robertson CI. 1982. The mechanics of two-dimensional cellular materials. *Proc Math Phys Eng Sci R Soc.* 382(1782):25–42.
- Gibson LJ, Ashby MF, Harley BA. 2010. *Cellular materials in nature and medicine.* Cambridge: Cambridge University Press.
- Gomberg BR, Saha PK, Wehrli FW. 2003. Topology-based orientation analysis of trabecular bone networks. *Med Phys.* 30(2):158–168.
- Hambli R. 2013. Micro-CT finite element model and experimental validation of trabecular bone damage and fracture. *Bone* 56(2):363–374.
- Hamed E, Jasiuk I, Yoo A, Lee Y, Liszka T. 2012. Multi-scale modelling of elastic moduli of trabecular bone. *J R Soc Interface.* rsif20110814.
- Hara T, Tanck E, Homminga J, Huiskes R. 2002. The influence of microcomputed tomography threshold variations on the assessment of structural and mechanical trabecular bone properties. *Bone* 31(1):107–109.
- Harrison NM, McDonnell PF, O'Mahoney DC, Kennedy OD, O'Brien FJ, McHugh PE. 2008. Heterogeneous linear elastic trabecular bone modelling using micro-CT attenuation data and experimentally measured heterogeneous tissue properties. *J Biomech.* 41(11):2589–2596.
- Hildebrand T, Rüegsegger P. 1997. Quantification of bone microarchitecture with the structure model index. *Comput Methods Biomech Biomed Eng.* 1(1):15–23.
- Homminga J, Van-Rietbergen B, Lochmuller EM, Weinans H, Eckstein F, Huiskes R. 2004. The osteoporotic vertebral structure is well adapted to the loads of daily life, but not to infrequent Berror loads. *Bone.* 34(3):510–516.
- Hou FJ, Lang SM, Hoshaw SJ, Reimann DA, Fyhrie DP. 1998. Human vertebral body apparent and hard tissue stiffness. *J Biomech.* 31(11):1009–1015.
- Imai K, Ohnishi I, Bessho M, Nakamura K. 2006. Nonlinear finite element model predicts vertebral bone strength and fracture site. *J Spine.* 31:1789–1794.
- Ito Y, Shum PC, Shih AM, Soni BK, Nakahashi K. 2006. Robust generation of high-quality unstructured meshes on realistic biomedical geometry. *Int J Numer Methods Eng.* 65(6):943–973.
- Jaasma MJ, Bayraktar HH, Niebur GL, Keaveny TM. 2002. Biomechanical effects of intraspecimen variations in tissue modulus for trabecular bone. *J Biomech.* 35:237–246.
- Jinnai H, Watashiba H, Kajihara T, Nishikawa Y, Takahashi M, Ito M. 2002. Surface curvatures of trabecular bone microarchitecture. *Bone* 30(1):191–194.
- Jones AC, Wilcox RK. 2007. Assessment of factors influencing finite element vertebral model predictions. *J Biomech Eng.* 129(6):898–903.
- Kabel J, van Rietbergen B, Odgaard A, Huiskes R. 1999. Constitutive relationships of fabric, density, and elastic properties in cancellous bone architecture. *Bone* 25(4):481–486.
- Keaveny TM, Borchers RE, Gibson LJ, Hayes WC. 1993. Trabecular bone modulus and strength can depend on specimen geometry. *J Biomech.* 26(8):991–1000.
- Keaveny TM, Pinilla TP, Crawford RP, Kopperdahl DL, Lou A. 1997. Systematic and random errors in compression testing of trabecular bone. *J Orthop Res.* 15(1):101–110.
- Keyak JH, Rossi SA, Jones KA, Skinner HB. 1997. Prediction of femoral fracture load using automated finite element modeling. *J Biomech.* 31(2):125–133.
- Ladd AJC, Kinney JH. 1998. Numerical errors and uncertainties in finite-element modeling of trabecular bone. *J Biomech.* 31:941–945.
- van Lenthe GH, Stauber M, Müller R. 2006. Specimen-specific beam models for fast and accurate prediction of human trabecular bone mechanical properties. *Bone* 39(6):1182–1189.
- Lü L, Meng G, Gong H, Zhu D, Gao J, Fan Y. 2015. Tissue level microstructure and mechanical properties of the femoral head in the proximal femur of fracture patients. *Acta Mech Sin.* 31(2):259–267.
- Luisier B, Dall'Ara E, Pahr DH. 2014. Orthotropic HR-pQCT-based FE models improve strength predictions for stance but not for sideways fall loading compared to isotropic QCT-based FE models of human femurs. *J Mech Behav Biomed Mater.* 32:287–299.
- Martin H, Werner J, Andresen R, Schober HC, Schmitz KP. 1998. Noninvasive assessment of stiffness and failure load of human vertebrae from CT-data. *Biomed Tech.* 43(4):82–88.
- Müller R, Rüegsegger P. 1995. Three-dimensional finite element modelling of non-invasively assessed trabecular bone structures. *Med Eng Phys.* 17(2):126–133.
- Nawathe S, Akhlaghpour H, Boussein ML, Keaveny TM. 2013. Microstructural failure mechanisms in the human proximal femur for sideways fall loading. *J Bone Miner Res.* 29:507–515.
- Niebur GL, Feldstein MJ, Yuen JC, Chen TJ, Keaveny TM. 2000. High-resolution finite element models with tissue strength asymmetry accurately predict failure of trabecular bone. *J Biomech.* 33:1575–1583.
- Pahr DH, Zysset PK. 2008. Influence of boundary conditions on computed apparent elastic properties of cancellous bone. *Biomech Model Mechanobiol.* 7(6):463–476.
- Pahr DH, Zysset PK. 2009. A comparison of enhanced continuum FE with micro FE models of human vertebral bodies. *J Biomech.* 42:455–462.

- Pahr DH, Zysset PK. 2016. Finite element-based mechanical assessment of bone quality on the basis of in vivo images. *Curr Osteoporos Rep.* 14(6):374–385.
- Pahr DH, Dall'Ara E, Varga P, Zysset PK. 2012. HR-pQCT-based homogenised finite element models provide quantitative predictions of experimental vertebral body stiffness and strength with the same accuracy as μ FE models. *Comput Methods Biomech Biomed Eng.* 15(7):711–720.
- Parkinson IH, Badiei A, Stauber M, Codrington J, Müller R, Fazzalari NL. 2012. Vertebral body bone strength: the contribution of individual trabecular element morphology. *Osteoporos Int.* 23(7):1957–1965.
- Perilli E, Baleani M, Öhman C, Fognani R, Baruffaldi F, Viceconti M. 2008. Dependence of mechanical compressive strength on local variations in microarchitecture in cancellous bone of proximal human femur. *J Biomech.* 41(2):438–446.
- Pioletti DP. 2010. Biomechanics in bone tissue engineering. *Comput Methods Biomech Biomed Engin.* 13(6):837–846.
- Pistoia W, van Rietbergen B, Laib A, Ruegsegger P. 2001. High-resolution three-dimensional-pQCT images can be an adequate basis for in-vivo μ FE analysis of bone. *J Biomech Eng.* 123(2):176–183.
- Rajan K. 1985. Linear elastic properties of trabecular bone: a cellular solid approach. *J Mater Sci Lett.* 4(5):609–611.
- van Rietbergen B, Weinans H, Huiskes R, Odgaard A. 1995. A new method to determine trabecular bone elastic properties and loading using micromechanical finite-element models. *J Biomech.* 28(1):69–81.
- Schileo E, Taddei F, Malandrino A, Cristofolini L, Viceconti M. 2007. Subject-specific finite element models can accurately predict strain levels in long bones. *J Biomech.* 40(13):2982–2989.
- Stauber M, Nazarian A, Müller R. 2014. Limitations of global morphometry in predicting trabecular bone failure. *J Bone Miner Res.* 29(1):134–141.
- Taddei F, Schileo E, Helgason B, Cristofolini L, Viceconti M. 2007. The material mapping strategy influences the accuracy of CT-based finite element models of bones: an evaluation against experimental measurements. *Med Eng Phys.* 29(9):973–979.
- Treece GM, Prager RW, Gee AH. 1999. Regularised marching tetrahedra: improved iso-surface extraction. *Comput Graph.* 23(4):583–598.
- Turner CH, Cowin SC, Rho JY, Ashman RB, Rice JC. 1990. The fabric dependence of the orthotropic elastic constants of cancellous bone. *J Biomech.* 23(6):549–561.
- Ulrich D, van Rietbergen B, Weinans H, Ruegsegger P. 1998. Finite element analysis of trabecular bone structure: a comparison of image-based meshing techniques. *J Biomech.* 31(12):1187–1192.
- Verhulp E, van Rietbergen B, Huiskes R. 2006. Comparison of microlevel and continuum-level voxel models of the proximal femur. *J Biomech.* 39(16):2951–2957.
- Verhulp E, Van Rietbergen B, Müller R, Huiskes R. 2008. Micro-finite element simulation of trabecular-bone post-yield behaviour—effects of material model, element size and type. *Comput Methods Biomech Biomed Eng.* 11(4):389–395.
- Viceconti M, Bellingeri L, Cristofolini L, Toni A. 1998. A comparative study on different methods of automatic mesh generation of human femurs. *Med Eng Phys.* 20(1):1–10.
- Viceconti M, Hunter P, Hose R. 2015. Big data, big knowledge: big data for personalized healthcare. *IEEE J Biomed Health.* 19(4):1209–1215.
- Wang J, Zhou B, Liu XS, Fields AJ, Sanyal A, Shi X, Adams M. 2015. Trabecular plates and rods determine elastic modulus and yield strength of human trabecular bone. *Bone* 72:71–80.
- Yosibash Z, Tal D, Trabelsi N. 2010. Predicting the yield of the proximal femur using high-order finite-element analysis with inhomogeneous orthotropic material properties. *Philos Trans A Math Phys Eng Sci.* 368(1920):2707–2723.
- Zysset PK. 2003. A review of morphology-elasticity relationships in human trabecular bone: theories and experiments. *J Biomech.* 36(10):1469–1485.
- Zysset PK, Dall'Ara E, Varga P, Pahr DH. 2013. Finite element analysis for prediction of bone strength. *Bone. Key reports,* 2.
- Zysset P, Pahr D, Engelke K, Genant HK, McClung MR, Kendler DL, Recknor C. 2015. Comparison of proximal femur and vertebral body strength improvements in the FREEDOM trial using an alternative finite element methodology. *Bone* 81:122–130.